Simulation of Yield-Stress Fluid in a Rotational Rheometer: The Effect of Vane Geometry on the Accuracy of Measured Properties

Angelica M. Oliva[1], Nathan R. Hargrave[1], Dimitri Feys[2] and Joontaek Park*[1]
[1]Chemical and Biochemical Engineering Department, Missouri University of Science & Technology, Rolla, MO, USA
[2]Civil, Architectural & Environmental Engineering Department, Missouri University of Science & Technology, Rolla, MO, USA
*Corresponding author: 110 Bertelsmeyer Hall, 1101 N. State St., Missouri S&T, Rolla, MO, 65409, USA, parkjoon@mst.edu

Abstract: A rotational rheometer for Self-Consolidating Concrete was simulated as a yield-stress fluid in a 2D geometry. The effect of the vane geometry was investigated by comparing the analytical solutions with the numerical output for flow in the coaxial cylinders. This effect was studied by investigating the torque vs rotational velocity relation, the flow pattern, and the shear stress distribution. The results show that the number of vane blades is crucial in the torque-rotational velocity relation whereas the vane curvature has minimal effect on the difference between the numerical results and the analytical equations. This study can suggest a design of an efficient rotational rheometer for cement-based materials as well as any yield-stress fluids.

Keywords: Self-consolidating concrete, cement-based materials, yield-stress fluid, rotational rheometer

1. Introduction

The flow of Self-Consolidating Concrete (SCC) in a rotational rheometer was simulated using COMSOL Multiphysics®. This study focuses on the effect of the vane geometry on the relation between the rotational velocity and the torque, from which the rheological properties can be calculated. Due to the importance of rheology in the use of SCC (no energy is required for consolidation [1]), enhancing the reliability of its rheological measurement is essential in its application.

Concrete is a construction material, mainly consisting of cement, sand, coarse aggregates and water. The complexity to study the rheology and flow of concrete is caused by the large range of particle sizes: from 100 nm up to 20 mm. Standard rheometers available to measure polymers and liquids are not suitable to measure the rheological properties of fresh concrete. Different large devices have been developed to accommodate large particles, the ICAR rheometer (developed at the International Center for Aggregate Research located at the University of Texas at Austin [2]) being one of them.

The ICAR rheometer consists of a large bucket (cylindrical container, R_o = 143 mm) with a vane with straight blades (R_i = 63.5 mm, H = 127 mm) (similar to Figure 1). By varying the rotational velocity and measuring the torque response at the inner, rotating vane, the rheological properties can be calculated. However, to calculate the rheological properties, it is assumed that the rheometer can be considered as a coaxial cylinders system. Recent numerical simulations have shown that this assumption is not valid, and that the real flow pattern causes inaccurate calculation of the rheological properties [3,4]. The purpose of this study is to improve the design of the inner cylinder of the ICAR rheometer by means of numerical simulations.

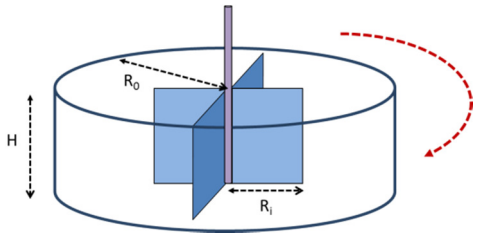

Figure 1. Schematic diagram of the rotational rheometer in this study. The cylindrical container (H: height, R_o: radius) rotates with an angular velocity of Ω which requires torque, T. A vane with 4 straight blades (R_i: blade length) are fixed at the rotating axis.

In this study, the SCC flow was assumed as a single phase yield-stress fluid (particles are ignored). The rheometer in this study is demonstrated in Figure 1. 2D rotational

geometry was chosen for simulating this rheometer. For convenience of simulation, the cylindrical container rotates in the simulation instead of the vane in reality. Whether the vane or outer cylinder rotates does theoretically not influence the shear stress and shear rate distribution. For a chosen set of fluid properties, the torque-rotational velocity relation will be investigated for different vane geometries.

2. Analytical Solution

The Bingham model describes the stress response of a yield-stress fluid under a simple shear flow as a linear function of shear rate with an intercept of yield stress, τ_y, and a slope of plastic viscosity, μ_p.

Rotational flows of yield-stress fluid also show the linear relation between Ω [rad/s] and T [Nm]. Whereas no analytical expression for yield-stress fluids in rheometers with blades as in Figure 1 is available, an analytical expression for fluids between two coaxial cylinders (instead of the vane, a stationary inner cylinder with radius R_i is used) can be found elsewhere [5]:

$$\frac{T}{H} = \frac{4\pi(R_o R_i)^2}{\left({R_o}^2 - {R_i}^2\right)}\left[\ln\left(\frac{R_o}{R_i}\right)\tau_y + 120\pi\mu_p \mathrm{N}\right] \quad (1)$$

Here, N is the rotational velocity with a unit of rpm (=30Ω/π). The end effect is neglected under an assumption of $H \gg R_o$. In our 2D simulation, torque per unit length of H, T/H, will be evaluated as a function of N (1.8 – 36 rpm) for various vane geometries under different properties. The simulation results will be compared with the analytical results from (1).

3. Simulation Methods

3.1 Governing Equations

The governing equations for this simulation are the continuity equation and the Cauchy momentum balance equation (ρ: fluid density, **u**: fluid velocity vector, t: time, p: pressure, **τ**: stress tensor, and **g**: gravity acceleration vector).

$$\frac{\partial \rho}{\partial t} = -\nabla \cdot (\rho \boldsymbol{u}) \quad (2)$$

$$\rho \frac{D\boldsymbol{u}}{Dt} = -\nabla p + \nabla \cdot \boldsymbol{\tau} + \rho \boldsymbol{g} \quad (3)$$

Since the yield-stress fluid is modeled as Bingham fluids, the constitutive equation for **τ** in (3) is given in terms of μ_p, τ_y, regularization parameter, ε, deformation tensor, $\Delta = \nabla \mathbf{u} + (\nabla \mathbf{u})^T$, and shear rate, $\dot{\gamma} = \sqrt{\frac{1}{2}\Delta : \Delta}$.

$$\boldsymbol{\tau} = \left(\mu_p + \frac{\tau_y}{\sqrt{\dot{\gamma}^2 + \varepsilon^2}}\right)\Delta \quad (4)$$

Note here that ε is commonly used for numerical simulation of Bingham fluids to avoid the singularity of (4) by imposing a minimum shear rate [6]. Due to ε, the stress-shear rate relation evaluated from (4) shows a deviation from the analytical expression of Bingham at very small shear rates (no intercept). Although the choice of very small ε results in negligibly small errors, convergent solutions are very difficult to achieve using typical Newton methods [6,7]. However, previous experience indicated that the Double dogleg method (with $\varepsilon = 10^{-15}$ s^{-1}) can result in convergent solutions significantly faster than the Newton method (with $\varepsilon < 10^{-6}$ s^{-1}).

3.2 Implementation in COMSOL

In the "Model Wizard" window, we chose "2D" as a space domain and "Fluid Flow/Single-Phase Flow/Rotating Machinery, Laminar Flow" as a physics model. This model is provided in the "Fluid Dynamics" module. "Preset Studies/ Frozen Rotor" was selected for evaluating steady state solutions in this study. We defined μ_p, τ_y, ε, and Ω as the global parameters.

The 2D representation of the rotating rheometer (Figure 1) was performed using the "Geometry" tools: the "Circle" for the container (R_o=0.02m), the "Bezier polygon" for the straight blade (R_i=0.0075m) and "Interpolation Curve" for the curved blades (e.g. turning point at x=0.001875, y=0.00375 for a blade has its tip at x=0, y=0.0075so that its curvature=640/3 m^{-1}). The shortest distance between the rotating axis and the tip of the blade is defined as R_i=0.0075m. Figure 2 demonstrates the rheometers with 4

straight blades and the 4 curved blades, respectively. In this study, 5 different geometries (4 and 12 straight blades; 4 and 12curved blades; and coaxial cylinders) are investigated for the study of the vane geometry effect. Note here that the scale of the rheometer in simulation was chosen to be (~ factor of 10) smaller than the actual scale. However, there is no effect of the scale-down on the resulting trends.

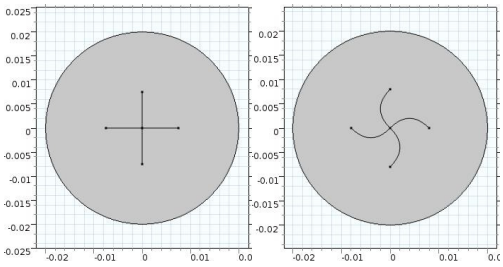

Figure 2. 2D representation of the rheometers with 4 straight blades (left) and 4 curved blades (right).

For the "Fluid Properties", the fluid density was chosen as ρ=2350 kg/m^3 as in a typical SCC and the dynamic viscosity, μ, was input as in (4) by choosing the "User-defined" model. The outer cylinder wall was set as the "Rotating wall" while the no-slip boundary conditions were imposed on the vanes in "Interior wall". Extra-fine physics-controlled mesh was applied to the entire fluid domain.

3.3 Simulation Procedure

First, a vane geometry was chosen among 5 different geometries (4 and 12 straight blades; 4 and 12 curved blades; and coaxial cylinders). Second, a set of the SCC properties was chosen from the list shown in Table 1. Third, numerical solutions for $1.8 \leq N \leq 36$rpm was evaluated using both the Double dogleg method and the (automatic highly nonlinear) Newton method as a solver option. If it is difficult to get a convergent solution within a given tolerance (usual for the cases of low N with the Newton method), the iteration was stopped at 200 steps. Note here that a severely oscillating or diverging relative error was never encountered. Finally, T/H was calculated both on the outer and inner cylinder surfaces using "Results/Derived Variables/Line Integral" for the product of the shear stress (=$\mu\dot{\gamma}$: rmspf.mu * rmspf.sr) and the lever arm R_o. Flow patterns were obtained by "2D surface" map of the flow magnitude (rmspf.U) and "2D Streamline" (u and v). Shear stress distributions were expressed using the "2D surface" map.

Table 1: Material properties of SCC used in this study

Material Properties	Concrete Type
τ_y=20Pa, μ_p=20Pa·s	SCC on the verge (lower limit) of instability
τ_y=20Pa, μ_p=100Pa·s	Very sticky SCC but with high flowability
τ_y=150Pa, μ_p=20Pa·s	Low viscous semi-flowable SCC

4. Results & Discussion

4.1. Coaxial Cylinders: The Effect of the Solver Method

(a) Evaluated on the outer cylinder surface

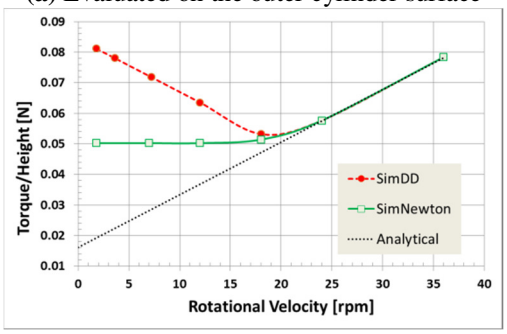

(b) Evaluated on the inner cylinder surface

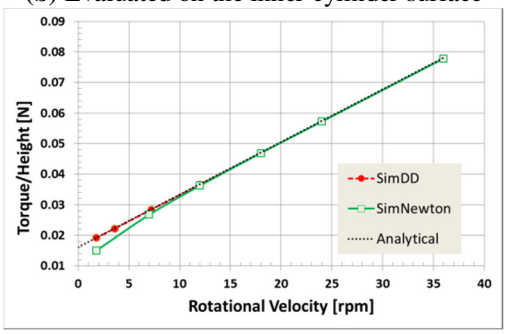

Figure 3. Evaluation of T/H as a function of N **(a)** on the outer cylinder and **(b)** on the inner cylinder. The material properties of SCC are τ_y=20Pa, μ_p=20 Pa·s.

Numerical solutions from the Double dogleg method and the Newton method are indicated as red and green, respectively. Analytical solution is shown as black.

The simulations were also performed using a coaxial cylinders system. Figure 3 shows the results of T/H vs N from the simulation of SCC with τ_y=20Pa, μ_p=20Pa·s. The numerical solutions from the Double dogleg method (red dashed line) and the Newton method (green straight line) are compared with the analytical solution (black dotted line). Figure 3a shows the torques evaluated on the outer cylinder. Both simulation results show huge discrepancy from the analytical solution at N<20rpm. However, the simulated torques on the inner cylinder show good agreement with the analytical solution (Figure 3b). The results from the Newton method show small numerical error at N<7rpm.

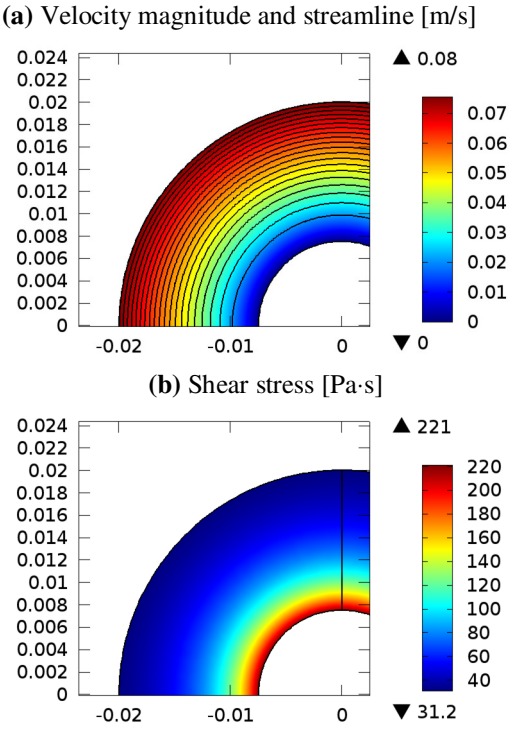

Figure 4. Simulation results of **(a)** the flow distribution map and **(b)** the shear stress map from the SCC of τ_y=20Pa, μ_p=20 Pa·s in a rheometer with coaxial cylinders under N=36rpm. The numerical solutions were obtained using the Double dogleg method. Note that the solutions obtained from the Newton method were almost identical to these results.

The abnormal trends observed for the solutions evaluated on the outer cylinder can be explained by comparing the flow and stress distributions. Figure 4 shows the flow and stress distributions at N=36 rpm, where all torque values from each method are in good agreement with the analytical solution. The flow velocity is the maximum at the outer cylinder surface and monotonically decreases towards the inner cylinder. The stress shows the opposite trend because it is related to $1/r^2$, and thus increases towards the inner cylinder due to the curvature. Note here that these distributions are very similar for both methods when N>20rpm.

However, the flow and stress distributions at N<20rpm are shown to be very different according to the solver method. Figures 5 and 6 compare the flow and the stress distributions from each method. The results from the Double dogleg method show abnormal behaviors (the velocity maximum and the stress minimum are not on the outer cylinder surface) while the Newton method results in physically plausible pattern, such as large unyielded zone (stress $\approx\tau_y$; indicated as dark blue region in Figure 6b)

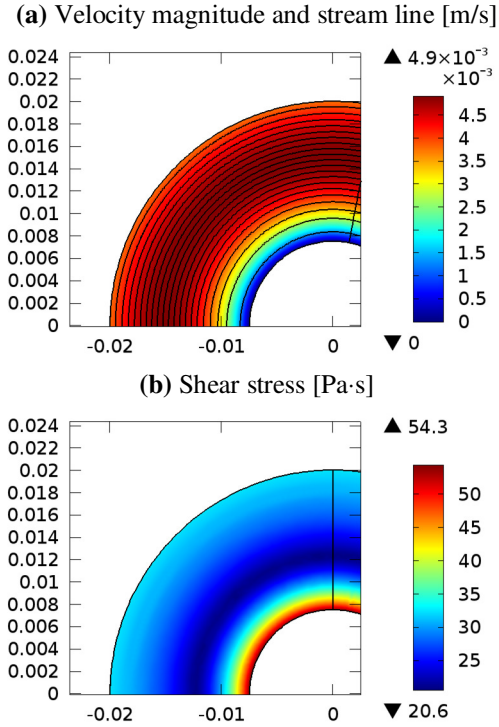

Figure 5. Simulation results of **(a)** the flow distribution map and **(b)** the shear stress map from the

SCC of τ_y=20Pa, μ_p=20 Pa·s in a rheometer with coaxial cylinders under N=1.8rpm. The numerical solutions were obtained using the Double dogleg method.

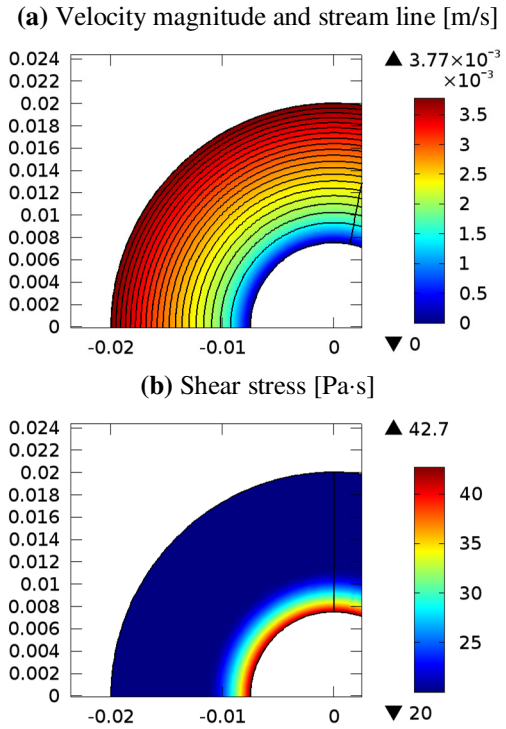

Figure 6. Simulation results of **(a)** the flow distribution map and **(b)** the shear stress map from the SCC of τ_y=20Pa, μ_p=20 Pa·s in a rheometer with coaxial cylinders under N=1.8rpm. The numerical solutions were obtained using the Newton method.

Note here that similar trends were observed for the simulation results from the other properties of SCC. The only difference was the change in the diverging points in Figure 3a. As μ_p increases compared to the value of τ_y, the diverging point happens at lower N (N=3.6rpm for τ_y=20Pa, μ_p=100Pa·s) while the SCC with high τ_y shows that point at a higher N (N=30rpm for τ_y=150Pa, μ_p=100Pa·s). This observation is in agreement with an increase in plug flow region with a decrease in N, and an increase in τ_y/μ_p.

In summary, the Double dogleg method results in the numerical solution which shows good agreement with the analytical torque evaluation in any range of N. However, this results in abnormal distributions of the physical values (flow and stress). Although the Newton method has disadvantages of difficulty in achieving convergent solution, it is recommended for getting the flow and the stress distributions which are physically plausible.

4.2. The Effect of the Vane Geometry

The simulations of flow in the rotational rheometer were performed with various vane geometries. Figure 7 shows the results of T/H vs N from the simulations of SCC with τ_y=20Pa, μ_p=100 Pa·s. Table 2 summarizes the intercepts and the slopes evaluated from each result. The numerical solutions are compared with the analytical solution of the coaxial cylinders.

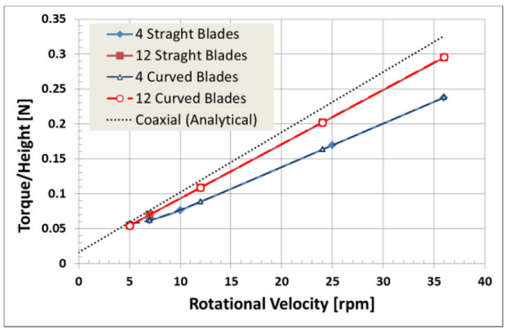

Figure 7. Evaluation of T/H as a function of N for various vane geometries (blue: 4 blades; red: 12 blades; black: analytical coaxial cylinders). The material properties of SCC are τ_y=20Pa, μ_p=100 Pa·s. Numerical solutions were obtained from the Double dogleg method. Note that the results from both the curved and the straight blades are almost identical.

Table 2: Intercepts and slopes evaluated from the results (at N>12rpm) in Figure 7

Case	Intercept	Slope
Coaxial	0.0161	0.00861
4 blades	0.0143	0.00622
12 blades	0.0158	0.00778

As reported in the previous study [4], the slope of the T/H-N line for the coaxial cylinders is higher than the slopes for any blades. The intercept (0.0161) of the T/H-N line for the coaxial cylinders is also higher (but very slightly) than those for 4 blades (~0.0143) and 12 blades (~0.0158). The T/H-N lines for the curved blades

and the straight blades were found to be almost identical. This clearly indicates that the T/H-N relation is not affected by the blade curvature. However, the number of blades affects the T/H-N relation. As the number of blades increases, the slope and the intercept get closer to those of the coaxial cylinders.

Those observed T/H-N trends be explained by comparing the flow patterns and the stress distributions of the different number and curvature of blades (Figure 8 - 10). The reduced slope of the T/H-N line for any blades is caused by the different flow and the stress patterns [4]. The flow patterns for the 4 blades (Figures 8a and 9a) show the square-like low flow velocity region near the rotating axis, which does not exist in the coaxial cylinders. Furthermore, the stress distributions of the 4 blades (Figures 8b and 9 b) show that most of the stress from the blades are exerted from the tip of each blade whereas the inner cylinder surface uniformly exerts stress to the surrounding fluids (Figures 4-6b).

(a) Velocity magnitude and stream line [m/s]

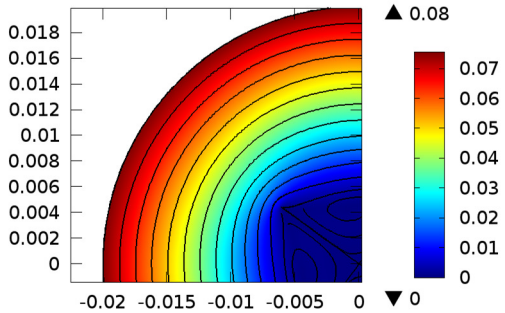

(b) Shear stress [Pa·s]

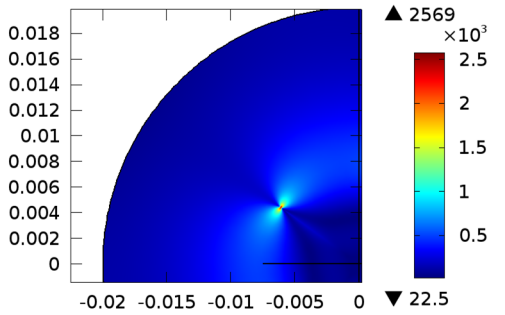

Figure 8. Simulation results of **(a)** the flow distribution map and **(b)** the shear stress map from the SCC of τ_y=20Pa, μ_p=100Pa·s in a rheometer with 4 straight blades under N=36rpm. The numerical solutions were obtained using the Double dogleg method.

The ineffectiveness of the blade curvature can be verified from comparing the flow and the stress maps in Figures 8 and 9, which look very similar. Regardless of the blade curvature, the flow velocities and the stress between blades are very low because the fluid is practically "trapped".

Comparison of Figures 8 and 10 suggests the explanation of the effect of the number of blades. The flow pattern in Figure 10 shows that the shape of the trapped-fluid region gets rounder with the increased number of blades. Additionally, the increased number of high-stress-exerting blade tips resulted in the increased T/H (slope) which is closer to that for the coaxial cylinders.

(a) Velocity magnitude and stream line [m/s]

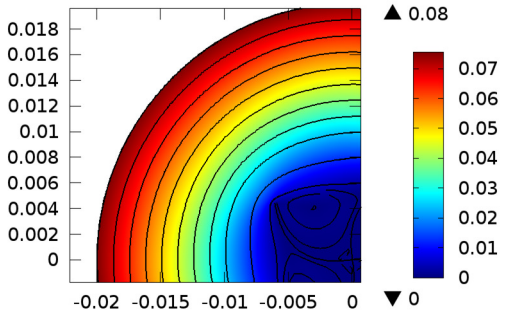

(b) Shear stress [Pa·s]

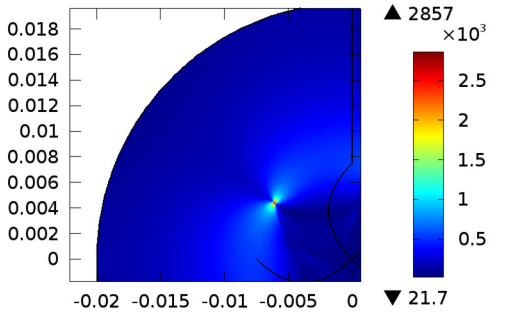

Figure 9. Simulation results of **(a)** the flow distribution map and **(b)** the shear stress map from the SCC of τ_y=20Pa, μ_p=100Pa·s in a rheometer with 4 curved blades under N=36rpm. The numerical solutions were obtained using the Double dogleg method.

(a) Velocity magnitude and stream line [m/s]

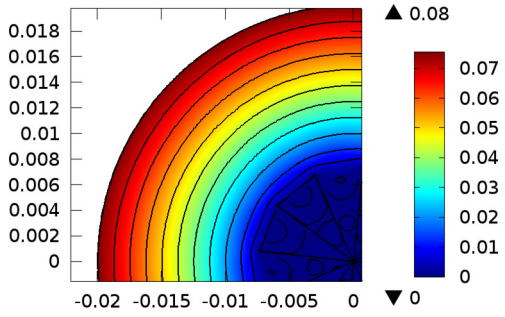

(b) Shear stress [Pa·s]

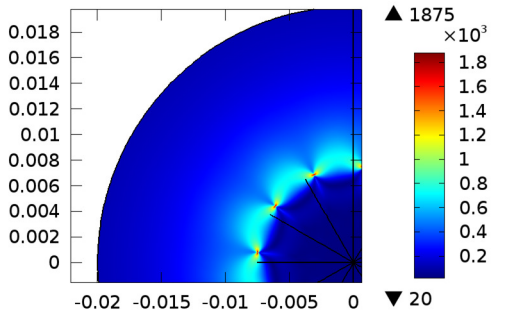

Figure 10. Simulation results of **(a)** the flow distribution map and **(b)** the shear stress map from the SCC of τ_y=20Pa, μ_p=100Pa·s in a rheometer with 12 straight blades under N=36rpm. The numerical solutions were obtained using the Double dogleg method.

5. Conclusions

The flow of SCC in the ICAR rheometer was simulated to study the effect of the vane geometry on the T/H-N relation. Additionally, the solver methods, specifically the Double dogleg and the Newton method were discussed by comparing the results from both methods. The Double dogleg method delivers the solution very quickly. However, non-physical solutions can be obtained for low N. The solutions from the Newton method seem more physically plausible, with the disadvantage of problems with converging solutions. The T/H-N relation was found to be independent of the blade curvature. However, as the number of the blades increases, the flow and the stress patterns get closer to those of the coaxial cylinders. Therefore, the findings from this study can be applied to the design of more efficient vane geometry. Future study on the other effects of the vane geometry, such as 3D structure and particle flow, as well as comparison with the experimental data is currently being performed.

6. References

1. De Schutter G., Bartos P., Domone P., Gibbs J., *Self-Compacting Concrete*, Whittles Publishing, Caithness (2008), 296pp.

2. http://www.germann.org/TestSystems/ICAR%20Rheometer/ICAR%20Rheometer.pdf

3. Zhu H, Martys N S, Ferraris C F, De Kee D, A Numerical Study of the Flow of Bingham-like Fluids in Two-Dimensional Vane and Cylinder Rheometers using a Smoothed Particle Hydrodynamics (SPH) based Method, *J non-Newton. Fluid Mech*. **165**, 362-375 (2010).

4. Wallevik J E, Effect of the Hydrodynamic Pressure on Shaft Torque for a 4-Blades Vane Rheometer, *Int. J. Heat Fluid Flow*, **50**, 95-102 (2014)

5. Feys D., Wallevik J. E., Yahia A., Khayat K. H., Wallevik O. H. Extension of the Reiner-Riwlin equation to determine modified Bingham parameters measured in coaxial cylinders rheometers, *Mater. Struct.* **46**, 289-311 (2013)

6. Denn M.M., Bonn D., "Issues in the flow of yield-stress liquids," *Rheol. Acta*, **50**, 307-315 (2011).

7. Alfi M., Benarjee N., Feys D., Park J. "Simulation of Formwork Filling by Cement Fluid: the Effect of the Formwork Structure on Yield-stress Fluid", The Proceedings of 2013 COMSOL Conference in Boston, http://www.comsol.com/paper/simulation-of-formwork-filling-by-cement-fluid-the-effect-of-the-formwork-struct-15135 (2013)

7. Acknowledgements

This work was supported by the Energy Research & Development Center at Missouri S&T (RDF85).